

Striped critical spin liquid in a spin-orbital entangled RVB state in a projected entangled-pair state representation

Piotr Czarnik¹ and Jacek Dziarmaga¹

¹*Instytut Fizyki Uniwersytetu Jagiellońskiego, ul. Reymonta 4, PL-30059 Kraków, Poland*

(Dated: June 20, 2014)

We introduce a spin-orbital entangled (SOE) resonating valence bond (RVB) state on a square lattice of spins- $\frac{1}{2}$ and orbitals represented by pseudospins- $\frac{1}{2}$. Like the standard RVB state, it is a superposition of nearest-neighbor hard-core coverings of the lattice by spin singlets, but adjacent singlets are favoured to have perpendicular orientations and, more importantly, an orientation of each singlet is entangled with orbitals' state on its two lattice sites. The SOE-RVB state can be represented by a projected entangled pair state (PEPS) with a bond dimension $D = 4$. This representation helps to reveal that the state is a superposition of striped coverings conserving a topological quantum number. The stripes are a critical quantum spin liquid. We propose a spin-orbital Hamiltonian supporting a SOE-RVB ground state.

PACS numbers: 75.25.Dk, 03.65.Ud, 03.67.Lx, 75.10.Kt

I. INTRODUCTION

Spin-orbital interplay is one of the most important topics in the theory of frustrated magnetism^{1–5}. When degenerate $3d$ orbitals in a transition metal oxide are partly filled, realistic superexchange includes both orbital and spin degrees of freedom that are strongly interrelated^{6,7}. In many cases, the intertwined spin-orbital interaction may be decoupled by mean field approximation, and the spin and orbital dynamics are independent from each other. Thus a spin-only Heisenberg model can be derived by averaging over the orbital state, which successfully explains magnetism and optical excitations in some materials, as for instance in LaMnO_3 ⁸. Recent interest and progress in the theory of spin-orbital superexchange models was triggered by the observation that orbital degeneracy drastically increases quantum fluctuations which may suppress long-range order in the regime of strong competition between different types of ordered states near a quantum critical point^{7,9}. Spin and orbital variables are here entangled.

The topological spin liquids (TSL) are at the forefront of condensed matter theory and quantum information¹³. They serve as an example of strongly correlated systems with non-Landau non-local order parameters. Their non-Abelian excitations can be used to operate a topological quantum computer^{10,11}. There are exactly solvable models with TSL ground states¹². The search for realistic models gained momentum after White demonstrated the TSL nature of the Kagome antiferromagnet¹³. This result was obtained by a tour-de-force application of the quasi-1D density matrix renormalization group, a technique elevated to a higher degree of sophistication in Ref.¹⁴. However, the use of DMRG in 2D is limited to systems with short-range correlations only, a restriction that does not apply to the PEPS ansatz¹⁵ whose usefulness for TSL has already been demonstrated^{16–18}, including doped RVB states¹⁹.

In this paper we introduce a spin-orbital entangled res-

onating valence bond (SOE-RVB) state on a square lattice with a spin-1/2 and orbital degrees of freedom represented by a pseudospin-1/2 at every lattice site. An orientation of each nearest-neighbor spin singlet along one of the lattice axes is entangled with the orbitals on its two lattice sites. The adjacent singlets are preferred to have perpendicular orientations as is often the case in the spin-orbital systems⁹. We use a PEPS representation of the SOE-RVB state to demonstrate that it is a striped topological quantum spin liquid with critical correlations.

The paper is organized as follows. In Section II, we introduce the SOE-RVB state on a square lattice. In Section III, we construct the PEPS representation of this state. In Section IV, the lattice is compactified to a cylinder of a finite circumference L and a transfer matrix along the cylinder is defined. In Section V, we introduce a simplification of the transfer matrix that is justified in the thermodynamic limit $L \rightarrow \infty$. In Section VI, the SOE-RVB state is shown to be a superposition of striped coverings that preserve a topological quantum number. In Section VII, correlations in the striped coverings are found to decay algebraically with a distance like in a critical state. In Section VIII, we introduce a toy spin-orbital Hamiltonian supporting the SOE-RVB state as a ground state, and a weak perturbation of the toy model that removes the degeneracy between different topological quantum numbers. In Section IX, a realistic Kugel-Khomskii Hamiltonian is shown to have the same energy in the SOE-RVB state as in the plaquette RVB state proposed earlier. Finally, we conclude in Section X. Some technical details were left for the appendix.

II. SOE-RVB STATE

At each lattice site of a 2D square lattice, in addition to a spin- $\frac{1}{2}$, there is a pseudospin- $\frac{1}{2}$ representing orbital degrees of freedom. The spin-orbital RVB state

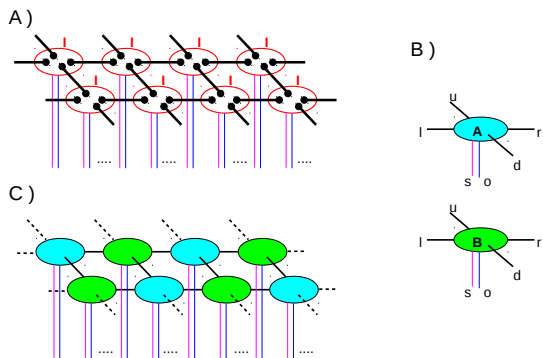


Figure 1. In A, the entangled-pair state (EPS) in (3) is placed on each bond connecting NN lattice sites. Then the isometry (projector) Z in (4) is applied at each site. In B, the projection creates at each site of the sublattice A or B a tensor A or B respectively. In C, the tensors contracted through their bond indices, but with free spin and orbital indices, make the PEPS representation of the SORVB state.

is a weighted sum over spin-singlet coverings

$$\sum_C w_C(\theta) |C\rangle. \quad (1)$$

It runs over all nearest-neighbor (NN) hard-core coverings, where each lattice site is covered by a NN spin-singlet. Each singlet is oriented from a sublattice A to B : $(|0_A\rangle|1_B\rangle - |1_A\rangle|0_B\rangle)/\sqrt{2}$. However, this state differs from the usual spin RVB state in two important respects:

- a horizontal(vertical) spin singlet is associated with an orbital state $|0_A 0_B\rangle(|1_A 1_B\rangle)$ on its two sites;
- the weights prefer pairs of adjacent singlets to be perpendicular to each other.

The entanglement between the singlet orientation and the orbitals' polarization is enough to make any two coverings that differ by just one pair of overlapping perpendicular singlets mutually orthogonal. The bias toward perpendicular adjacent singlets is effected by the weights $w_C(\theta) = \cos^K \theta$, where the parameter $\theta \in [0, \pi/2)$ and K is a number of NN lattice bonds connecting parallel singlets. When $\theta = 0$ we recover the standard orthogonal dimer state, but here we are more interested in the opposite limit $\theta \rightarrow \pi/2$, when parallel singlets are suppressed as much as possible, even though they cannot be quite eliminated. We study this limit in the PEPS representation.

III. PEPS REPRESENTATION

We define two states in an auxiliary Hilbert space:

$$\begin{aligned} |a\rangle &= |2\rangle \cos \frac{\theta}{2} + |3\rangle \sin \frac{\theta}{2}, \\ |b\rangle &= |2\rangle \cos \frac{\theta}{2} - |3\rangle \sin \frac{\theta}{2}, \end{aligned} \quad (2)$$

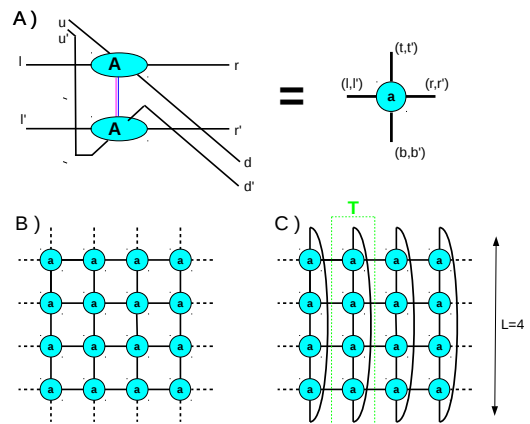


Figure 2. In A, a contraction of the PEPS tensor A with its conjugate through the spin and orbital indices makes a transfer tensor a . The same a is obtained on the sublattice B after contraction of the tensor B with its conjugate. In B, a norm squared of the PEPS is represented by a contraction of the transfer tensors. In C, the norm squared of the PEPS on a periodic cylinder of circumference $L = 4$. A contraction of all transfer tensors a in a periodic column makes a transfer matrix T .

with a product $(a|b) = \cos \theta$. On each bond connecting NN sites we place a virtual entangled-pair state (EPS)

$$|0_A 1_B\rangle - |1_A 0_B\rangle + |2_A 2_B\rangle + |3_A 3_B\rangle, \quad (3)$$

see Figure 1A. Then at each lattice site we apply an isometry (projector)

$$I = \sum_{i=0,1} |i_S 0_O\rangle [(a_U i_R b_D a_L] + (a_U b_R b_D i_L] + |i_S 1_O\rangle [(b_U a_R i_D b_L] + (i_U a_R a_D b_L]. \quad (4)$$

Here S, O refer to the spin and orbital on the site and U, R, B, L to the bonds coming out from it: L, R along the a -axis and U, D the b -axis. A resulting projected-EPS (PEPS) tensor on the sublattice A is

$$A_{u,r,d,l}^{s,o} = \delta_{o0} (u|a)(d|b) [(l|a)\delta_{rs} + \delta_{ls}(r|b)] + \delta_{o1} (l|b)(r|a) [\delta_{us}(d|a) + (u|b)\delta_{ds}] \quad (5)$$

Here the bond indices $u, r, d, l \in \{0, 1, 2, 3\}$ (the PEPS bond dimension $D = 4$) and the spin and orbital indices $s, o \in \{0, 1\}$. A PEPS tensor on the sublattice B is

$$B_{u,r,d,l}^{s,o} = (-1)^s \sum_{s'} \sigma_{s,s'}^x A_{u,r,d,l}^{s',o}. \quad (6)$$

A director $|a\rangle$ or $|b\rangle$ sticking out of a PEPS tensor along one of its bonds signals to its environment the orientation of a singlet covering its site. Each bond connecting parallel singlets is suppressed by a factor $(a|b) = \cos \theta$.

IV. TRANSFER MATRIX

To calculate its expectation value an operator has to be sandwiched between two PEPS's in Figure (1)C. In

the “sandwich” each PEPS tensor on a site that does not belong to the support of the operator is contracted with its conjugate through their spin and orbital indices, see Figure 2A. This contraction makes a transfer tensor a . Comparing (5) and (6) one finds that the transfer tensor is the same on both sublattices. The norm squared of the PEPS is represented in Figure 2B. In Figure 2C, the same norm is shown on a periodic cylinder of circumference L . A contraction of L transfer tensors in each periodic column makes a transfer matrix T .

V. DIAGONAL ENSEMBLE

The norm squared in Fig. 2C is a sum $\sum_{C,C'} w_C(\theta)w_{C'}(\theta)\langle C|C'\rangle$. For the overlap $\langle C|C'\rangle$ to be 0 it is enough that the coverings C and C' differ by just a single pair of perpendicular SOE singlets that overlap on a common site. The only way that two different coverings can have a non-zero overlap is that both coverings have a 1D train of singlets along the same line of sites, but the trains are shifted with respect to each other by one lattice site. However, with increasing system size the overlap between the shifted trains tends to zero exponentially fast. Since we are primarily interested in an extrapolation to the thermodynamic limit, in the following we approximate

$$\sum_{C,C'} w_C(\theta)w_{C'}(\theta)\langle C|C'\rangle \approx \sum_C w_C^2(\theta) \quad (7)$$

ignoring any overlaps between different coverings.

This “diagonal” approximation simplifies radically the transfer tensor a in Figure 2A. Instead of $D^2 = 16$ different values, each of its four bond indices can take only 3 values numbering an orthonormal basis in a subspace spanned by the following states

$$|aa\rangle, |bb\rangle, (|00\rangle + |11\rangle)/\sqrt{2} \quad (8)$$

with the last one indicating a singlet along a given bond. The three states become orthonormal when $\theta \rightarrow \pi/2$. The reduced bond dimension accelerates contraction of tensor networks like the one in Fig. 2C.

Some further reductions follow from the fact that the singlet can stick out only from one of the four indices of the transfer tensor a , i.e., if one index shows the singlet, then the other indices must show either $|aa\rangle$ or $|bb\rangle$. These correlations help to compactify the column transfer matrix T .

VI. TOPOLOGICAL STRIPE COVERINGS

The tensor network in Fig. 2C, corresponding to an infinite cylinder, is a graphic representation of an infinite power of the transfer matrix: T^N with $N \rightarrow \infty$. When a finite segment of length l of the infinite cylinder is concerned, then instead of the infinite power one can

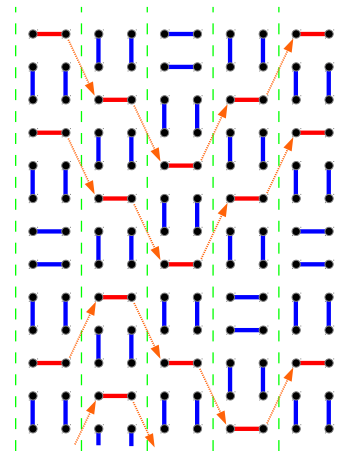


Figure 3. A typical singlet covering in the striped spin liquid. Here the black dots are lattice sites and the thick connecting lines represent spin singlets. The green dashed lines separate different stripes. The unpaired singlets are highlighted red. The orange arrows indicate their jumps between NN stripes.

consider a finite object $(L|T^l|R)$, where $(L|$ and $|R)$ are respectively the left and right dominant eigenvectors of T . The compact object $(L|T^l|R)$ can be used to scrutinize directly what singlet coverings appear in the finite segment and what are their probabilities. The direct scrutiny was completed up to $L = 12$. In the limit $\theta \rightarrow \pi/2$ only striped coverings survive, like the typical example in Fig. 3, with either vertical or horizontal orientation of the stripes. The following Table shows a relative weight of vertical stripes versus all coverings as a function of θ for $L = 11$.

$\theta/\frac{\pi}{2}$	weight
0.70	0.5002
0.80	0.7959
0.90	0.9809
0.92	0.9920
0.95	0.9988

For the sake of definiteness, in the following we focus on vertical stripes like in Fig. 3. The minimization of the number of bonds connecting parallel singlets in the limit $\theta \rightarrow \pi/2$ leads to an interesting topological conservation law. All singlets appear in parallel pairs, except for some unpaired horizontal singlets. The number of unpaired singlets in each vertical stripe is the same. This is a topologically protected quantum number. Only locations of singlets can change when passing between NN vertical stripes, but their total number remains the same. Each singlet jumps two lattice sites either up or down along a stripe, but with a constraint that two unpaired singlets cannot end at NN locations or, equivalently, they cannot be swapped along the stripe. Locations of consecutive unpaired singlets along a stripe differ by $3+4j$ sites with $j = 0, 1, 2, \dots$

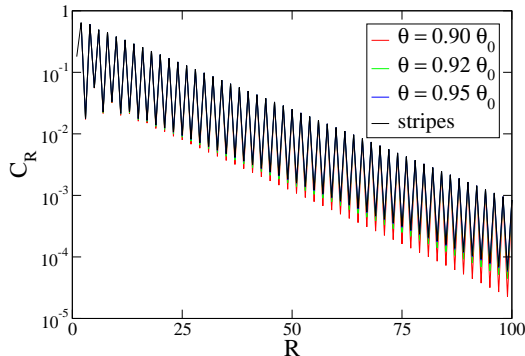


Figure 4. The absolute value of the correlator C_R in (12) along a cylinder with a circumference $L = 10$. With $\theta \rightarrow \frac{\pi}{2}$ the correlator obtained with the full transfer matrix T converges to the correlator in the striped state obtained with T_S . Here the dominant eigenvector of T_S has $\mathcal{N} = 2$ unpaired singlets. The exponential decay of C_R with R can be fitted with a correlation length $\xi \approx 15$.

VII. CORRELATIONS

Since a vertical (horizontal) singlet is associated with the orbital state $|11\rangle$ ($|00\rangle$), then an orbital operator

$$Z = |1\rangle\langle 1| - |0\rangle\langle 0| \quad (9)$$

can be conveniently used to characterize singlet correlations. Its average,

$$\langle Z \rangle = \mathcal{N}/L, \quad (10)$$

is a fraction of unpaired singlets. The following Table shows its convergence with $\theta \rightarrow \frac{\pi}{2}$ for $\mathcal{N} = 2, L = 6$.

$\theta/\frac{\pi}{2}$	$\langle Z \rangle$
0.90	0.333040
0.95	0.333315
0.97	0.333331

Correlators $\langle Z_i Z_j \rangle$ can be obtained either from the full transfer matrix T or the striped coverings only. With the last method one can reach longer L . When the unpaired singlets are represented by hard-core bosons, then the “striped” transfer matrix for \mathcal{N} particles becomes

$$T_S = P : \left(\sum_{l=1}^L c_{l+2}^\dagger c_l + \text{h.c.} \right) : P. \quad (11)$$

Here l is a location along a periodic stripe, c_l is a hard-core bosonic annihilation operator, and P is a projector enforcing the constraint that consecutive occupied locations differ by $3 + 4j$. An application of T_S to a Fock state with \mathcal{N} particles on L sites creates a superposition of Fock states with each particle shifted by ± 2 sites with respect to its original location.

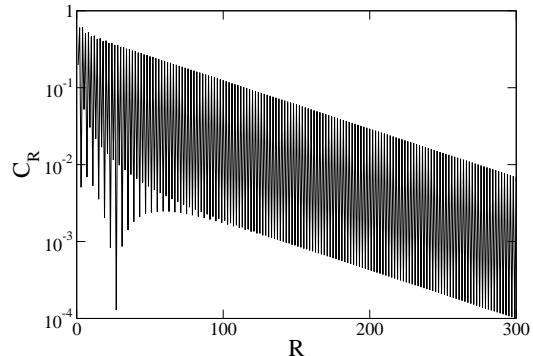


Figure 5. The absolute value of the correlator C_R in (12) along a cylinder with circumference $L = 72$ obtained with T_S in the striped state. Here the dominant eigenvector of T_S has $\mathcal{N} = 16$ unpaired singlets. The exponential decay of C_R with R can be fitted with a correlation length $\xi \approx 70$.

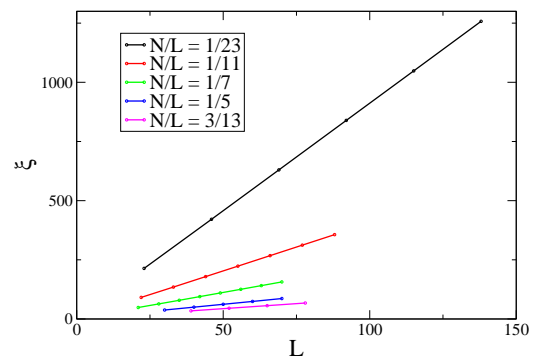


Figure 6. The correlation length ξ of the correlator C_R along a cylinder as a function of the cylinder’s circumference L obtained with T_S in the striped state for different values of the density \mathcal{N}/L of unpaired singlets. $\xi(L)$ proves to be a linear function. Its slope decreases with the density. The linearity proves that the transfer matrix T_S has a gap between its two most dominant eigenvalues that decays like $1/L$. The gap increases with the density of unpaired singlets.

Figure 4 shows a correlator

$$C_R = \langle Z_1 Z_{1+R} \rangle - \langle Z \rangle^2 \quad (12)$$

in the direction perpendicular to the stripes along a cylinder with a circumference $L = 10$. When $\theta \rightarrow \frac{\pi}{2}$ the correlators obtained with the full transfer matrix T converge to the correlator in the striped phase obtained with T_S . Figure 5 shows the same correlator in the striped state along a cylinder with a large circumference $L = 72$. For large R both correlators in Figs. 4 and 5 decay exponentially, but with a correlation length ξ that depends on L . In Figure 6 we make a systematic study of this size dependence. ξ proves to be a linear function of L whose slope decreases with increasing density of unpaired singlets \mathcal{N}/L . We can conclude that in the thermodynamic

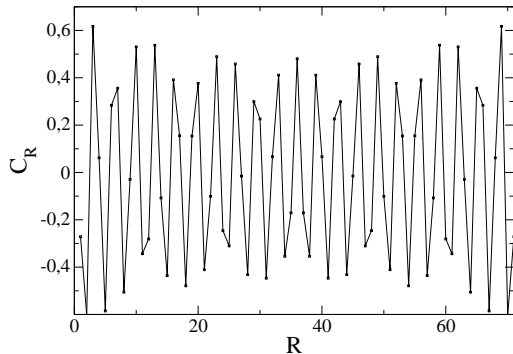


Figure 7. The correlator C_R in (12) along the stripes of length $L = 72$ with the dominant $\mathcal{N} = 16$. The correlator's decay with R is not significant.

limit $L \rightarrow \infty$ the decay of correlations in the direction perpendicular to the stripes is slower than exponential. Furthermore, since ξ^{-1} is a gap between the two most dominant eigenvalues of T_S , then this gap decays like $1/L$. The ‘‘Hamiltonian’’ T_S has ‘‘low energy’’ excitations with a linear dispersion relation.

The real symmetric T_S can be normalized to have the dominant eigenvalue $\Lambda_0 = 1$. With a spectral representation $T_S = \sum_m \Lambda_m |m\rangle\langle m|$ the correlator in the direction perpendicular to the stripes becomes

$$C_{2R+2}^\perp = \langle 0|ZT_S^R Z|0\rangle - \langle 0|Z|0\rangle^2 = \sum_{m>0} \langle 0|Z|m\rangle^2 \Lambda_m^R. \quad (13)$$

For the gapless excitations we have $|\Lambda_m| \approx 1 - \lambda_m/L$ and, for a large R , $\Lambda_m^R \approx (\pm 1)^R e^{-\lambda_m R/L}$. Taking $L \rightarrow \infty$ and replacing the sum over m with an integral over λ we obtain

$$C_{2R+2}^\perp \approx \int_0^\infty \frac{d\lambda}{L} \sigma(\lambda/L) z(\lambda/L) e^{-\lambda R/L}. \quad (14)$$

Here $\sigma(\dots)$ is density of states and $z(\dots)$ is an average value of $\langle 0|Z|m\rangle^2$. For a large R when small λ/L dominate

$$C_{2R+2}^\perp \sim R^{-(\gamma+1)}. \quad (15)$$

Here γ is an exponent in $\sigma(\lambda/L)z(\lambda/L) \sim (\lambda/L)^\gamma$ for small λ/L .

A numerical study in Figure 7 shows that the same correlator but in the direction along a stripe does not decay much within the numerically achievable distance. This is not quite unexpected given the gapless spectrum of T_S that implies a power-law decay of the correlator. This critical decay can be better understood in the regime of low density ρ of unpaired singlets, where the detailed microscopic form of the constraint P is irrelevant and the singlets can be replaced by a Tonks gas of impenetrable hard-core bosons. Furthermore, the correlator C_R between sites, say, l and $l + R$ depends only on a number of hard-core bosons on the sites $l + 1, \dots, l + R - 1$. A

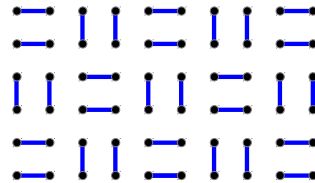


Figure 8. The plaquette RVB (PVB) state⁹. This is the special stripe covering without any unpaired singlets, $\mathcal{N} = 0$.

probability distribution for this number can be equivalently, and more conveniently, obtained from the Fermi sea with the same density of particles. As shown in detail in the Appendix, its variance is logarithmic in R , hence C_R decays as a power law:

$$C_R \sim (\rho R)^{-1/8} \cos \frac{\pi}{2}(\rho + 1)R. \quad (16)$$

The small exponent may explain the modest decay observed in Fig. 7.

VIII. SIMPLE HAMILTONIAN

Let us consider a toy spin-orbital Hamiltonian

$$H_0 = \lambda \sum_{\langle i,j \rangle} Z_i Z_j + \sum_{\langle i,j \rangle \parallel \gamma} \mathbf{S}_i \mathbf{S}_j \left(\frac{1 \mp Z_i}{2} \right) \left(\frac{1 \mp Z_j}{2} \right). \quad (17)$$

Here $\mathbf{S}_i = \frac{1}{2}\sigma_i$ are spin operators and Z_i orbital Pauli matrices. The upper(lower) signs correspond to a bond along $\gamma = a(b)$. Note that Z_i are good quantum numbers.

When $\lambda < \frac{3}{4}$ the energy of an isolated bond is minimized by a product of a spin singlet and an orbital ZZ -ferromagnet: $|00\rangle$ for a bond along a and $|11\rangle$ along b . This is just the SOE singlet in the SOE-RVB state.

Back on the lattice, we need $\lambda < \frac{3}{16}$ for the regular PVB covering in Figure 8 to have lower energy than the orbital Neel state. In the PVB state the adjacent singlets were made perpendicular as often as possible to minimize the energy of the λ -coupling between them. What is more, PVB is degenerate with all stripe coverings like the one in Fig. 3. It is the special stripe covering without any unpaired singlets, $\mathcal{N} = 0$.

However, for the stripes to be the ground states, λ must be also bounded from below. Indeed, when all $Z_i = -1(+1)$ are the same, then the λ -term contributes the energy of 2λ per site and the other term becomes 1D spin Heisenberg chains along the $a(b)$ -axis. Their ground state has energy -0.444 per site. The total energy of the 1D Heisenberg phase is $-0.444 + 2\lambda$. It is higher than the stripe energy $-3/8$ when $\lambda > 0.0345$. In conclusion, when $\lambda \in (0.0345, 3/16)$ the SOE-RVB belongs to the ground state manifold of H_0 .

Interestingly, the degeneracy of the stripes with different \mathcal{N} can be removed by a simple perturbation

$$V = g \sum_i X_i. \quad (18)$$

Here $X = |0\rangle\langle 1| + |1\rangle\langle 0|$ is an orbital Pauli matrix. A second order perturbative calculation shows that for $\lambda > 0.0625$ each unpaired singlet adds a negative contribution to the energy of the ground state making larger \mathcal{N} more favorable.

IX. KUGEL-KHOMSKII MODEL

A realistic version of the toy model (17) is a 2D Kugel-Khomskii model. The perturbation theory for a Mott insulator with active e_g orbitals in the regime of $t \ll U$ leads to the spin-orbital model²⁰

$$H = -\frac{1}{2}J \sum_{\langle ij \rangle || \gamma} \left\{ \left(r_1 \Pi_t^{(ij)} + r_2 \Pi_s^{(ij)} \right) \left(\frac{1}{4} - \tau_i^\gamma \tau_j^\gamma \right) + (r_3 + r_4) \Pi_s^{(ij)} \left(\frac{1}{2} - \tau_i^\gamma \right) \left(\frac{1}{2} - \tau_j^\gamma \right) \right\} - E_z \sum_i \tau_i^c, \quad (19)$$

The model describes the spin-orbital superexchange in K_2CuF_4 ²¹ with $J = 4t^2/U$. The terms proportional to $r_1 \equiv 1/(1-3\eta)$, $r_2 = r_3 \equiv 1/(1-\eta)$, and $r_4 \equiv 1/(1+\eta)$ refer to the charge excitations to the upper Hubbard band²⁰ which depend on Hund's exchange parameter $\eta = \frac{J_H}{U}$. The spin projection operators

$$\Pi_s^{(ij)} = \left(\frac{1}{4} - \mathbf{S}_i \cdot \mathbf{S}_j \right), \quad \Pi_t^{(ij)} = \left(\frac{3}{4} + \mathbf{S}_i \cdot \mathbf{S}_j \right). \quad (20)$$

select, respectively, a singlet or triplet configuration for spins $S = 1/2$ on the bond $\langle ij \rangle$.

Here τ_i^γ act in the subspace of e_g orbitals occupied by a hole $\{|x\rangle, |z\rangle\}$, with $|z\rangle \equiv (3z^2 - r^2)/\sqrt{6}$ and $|x\rangle \equiv (x^2 - y^2)/\sqrt{2}$ — they can be expressed in terms of Pauli matrices as²⁰:

$$\tau_i^{a(b)} \equiv \frac{1}{4} \left(-X_i \pm \sqrt{3}Z_i \right), \quad \tau_i^c = \frac{1}{2} X_i. \quad (21)$$

Finally, E_z is the crystal field splitting of two e_g orbitals, induced by the lattice geometry or pressure.

At small enough η and a suitable $E_z < 0$, the PVB state was argued⁹ to be a ground state of (19). At $\eta = 0$ its energy is

$$\langle \text{PVB} | H | \text{PVB} \rangle = -\frac{3(23 + 4\sqrt{3})}{128} JN = -0.7014JN, \quad (22)$$

where N is the number of lattice sites. It is straightforward, though cumbersome, to check that any striped covering has the same energy as the PVB state.

X. CONCLUSION

The spin-orbital entangled resonating-valence-bond state was shown to be a quantum superposition of striped spin-singlet coverings that conserve a topological quantum number equal to the number of unpaired singlets in a periodic stripe. Its correlations are critical. The SOE-RVB state is a ground state of a simple spin-orbital Hamiltonian. It has the same energy as the PVB state in the realistic 2D Kugel-Khomskii Hamiltonian.

ACKNOWLEDGMENTS

This work was supported by the Polish National Science Center (NCN) under Project DEC-2013/09/B/ST3/01603.

APPENDIX: CORRELATIONS ALONG A STRIPE FOR A LOW DENSITY OF UNPAIRED SINGLETS

For a given stripe covering C , the correlator $\langle Z_l Z_{l+R} \rangle_C$ along a stripe depends on a number n of unpaired singlets between the sites l and $l+R$ as

$$\langle Z_l Z_{l+R} \rangle_C = \begin{cases} 1 & \text{if } R+n+e = 0, 1, 4, 5, 8, 9, \dots \\ -1 & \text{if } R+n+e = 2, 3, 6, 7, 10, 11, \dots \end{cases}.$$

Here $e = 0, 1$ depending on the highest site number $l' \leq l$ occupied by an unpaired singlet. $e = 1(0)$ when $l - l'$ is even(odd). Since in the dilute limit e is equally likely to be 0 or 1, then only contributions of coverings with even $R+n$ survive in $\langle Z_l Z_{l+R} \rangle$. In other words, a surviving contribution of a covering C is

$$\begin{aligned} \langle Z_l Z_{l+R} \rangle_C^{\text{surv}} &= \begin{cases} 1 & \text{if } R+n = 0, 4, 8, 12, \dots \\ -1 & \text{if } R+n = 2, 6, 10, 14, \dots \\ 0 & \text{otherwise} \end{cases} \\ &= \cos \left[\frac{\pi}{2} (R+n) \right]. \end{aligned} \quad (23)$$

The correlator is an average over n :

$$C_R = \langle Z_l Z_{l+R} \rangle = \sum_{n=0}^{R-1} p_n \cos \left[\frac{\pi}{2} (R+n) \right]. \quad (24)$$

Here p_n is a probability distribution for n .

The striped transfer matrix (11) is written in the language of hard-core bosons. As long as only coarse-grained features of its leading eigenvector, like the distribution p_n between distant sites, are concerned in the regime of low density, the constraint imposed by the projector P can be relaxed. It affects only fine details of the wave function on the scale comparable to the lattice constant. By

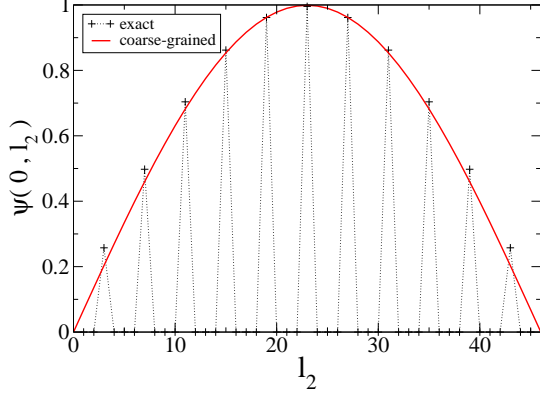


Figure 9. The leading eigenvector of the striped transfer matrix T_S for $\mathcal{N} = 2$ unpaired singlets on $L = 46$ sites. The plots compare the exact leading eigenfunction $\psi(0, l_2)$ of the exact T_S in Eq. (11) with its coarse-grained counterpart in Eq. (26). Both functions are in arbitrary units. The coarse-grained eigenfunction captures accurately the envelope of the exact one.

the same token, the next-NN hopping can be replaced by a NN hopping so that the transfer matrix becomes

$$T_S \approx : \left(\sum_{l=1}^L c_{l+1}^\dagger c_l + \text{h.c.} \right)^\mathcal{N} : . \quad (25)$$

An application of this T_S to a Fock state with \mathcal{N} particles creates a superposition of Fock states with each particle shifted by ± 1 lattice site with respect to its original location. In other words, a repeated application of T_S generates a \mathcal{N} -particle random walk of particles constrained not to occupy the same site. The \mathcal{N} -particle probability distribution describing the stochastic process converges with time to a stationary one:

$$\psi(l_1, \dots, l_\mathcal{N}) = \prod_{i < j} \sin \left(\frac{\pi |l_i - l_j|}{L} \right). \quad (26)$$

An accuracy of this coarse-grained approximation can be appreciated in Figure 9. Interestingly, this coarse-grained leading eigenvector of T_S is the ground state of the 1D Tonks gas of hard-core bosons.

In the dilute regime, p_n is a probability to find n particles between the sites l and $l + R$ in the state (26). p_n does not change when we replace the hard-core bosons with fermions²² and the state (26) with a Fermi sea of \mathcal{N} particles on L sites. For fermions the characteristic function of p_n ,

$$\chi_\lambda = \sum_{n=0}^{R-1} p_n e^{i\lambda n}, \quad (27)$$

is known²³ for a large block of length $R \rightarrow \infty$ in an

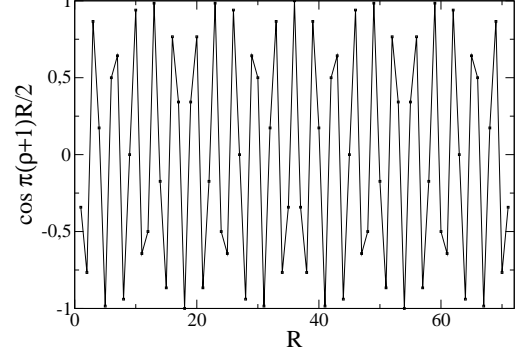


Figure 10. The oscillating part of the analytic correlator (29) along a periodic stripe of length $L = 72$ for $\mathcal{N} = 16$ unpaired singlets and a singlet density $\rho = \mathcal{N}/L = 16/72$. These parameters are the same as in Fig. 7. In both Figures the fast oscillations are the same.

infinite system:

$$\chi(\lambda) = G^2(1 + \lambda/2\pi)G^2(1 - \lambda/2\pi) \times e^{i\lambda\rho R} (2R \sin \pi\rho)^{-\lambda^2/2\pi^2}. \quad (28)$$

Here ρ is a particle density and G denotes the G-Barnes function.

In general $R = 4r + \delta$, where r is an integer and $\delta = 0, 1, 2, 3$ is a remainder. Since in the dilute limit the probabilities p_n for n close to $R - 1$ are exponentially small, we can proceed with Eq. (24) as follows:

$$\begin{aligned} C_R &= \sum_{n=0}^{4r+\delta-1} p_n \cos \frac{\pi}{2}(4r + \delta + n) \\ &\approx \sum_{n=0}^{4r-1} p_n \cos \frac{\pi}{2}(\delta + n) \\ &= \frac{\chi_{\frac{\pi}{2}} + \chi_{-\frac{\pi}{2}}}{2} \cos \frac{\pi\delta}{2} - \frac{\chi_{\frac{\pi}{2}} - \chi_{-\frac{\pi}{2}}}{2i} \sin \frac{\pi\delta}{2} \\ &\sim (\rho 4r)^{-1/8} \left(\cos \frac{\pi\rho 4r}{2} \cos \frac{\pi\delta}{2} - \sin \frac{\pi\rho 4r}{2} \sin \frac{\pi\delta}{2} \right) \\ &= (\rho 4r)^{-1/8} \cos \frac{\pi}{2}(\rho 4r + \delta) \\ &\approx (\rho R)^{-1/8} \cos \frac{\pi}{2}(\rho + 1)R. \end{aligned} \quad (29)$$

The correlator along a stripe decays slowly with the exponent $1/8$. This may explain the modest decay with R observed in Fig. 7.

Remarkably, the low density formula (29) captures correctly the fast oscillations in Fig. 7. Indeed, in Fig. 10 the function $\cos \frac{\pi}{2}(\rho + 1)R$ is shown for a stripe of length $L = 72$ and the density of unpaired singlets $\rho = 16/72$ just like in Fig. 7. The fast oscillations in both Figures are the same.

-
- ¹ Y. Tokura and N. Nagaosa, *Science* **288**, 462 (2000).
- ² J. van den Brink, Z. Nussinov, and A.M. Oleś, in: *Introduction to Frustrated Magnetism: Materials, Experiments, Theory*, edited by C. Lacroix, P. Mendels, and F. Mila (Springer, New York, 2011).
- ³ G. Khaliullin, *Prog. Theor. Phys. Suppl.* **160**, 155 (2005).
- ⁴ A. M. Oleś, G. Khaliullin, P. Horsch, and L. F. Feiner, *Phys. Rev. B* **72**, 214431 (2005).
- ⁵ A. M. Oleś, *J. Phys.: Condens. Matter* **24**, 313201 (2012).
- ⁶ K. I. Kugel and D. I. Khomskii, *Sov. Phys. Usp.* **25**, 231 (1982).
- ⁷ L. F. Feiner, A. M. Oleś, and J. Zaanen, *Phys. Rev. Lett.* **78**, 2799 (1997); *J. Phys.: Condens. Matter* **10**, L555 (1998); G. Khaliullin and V. Oudovenko, *Phys. Rev. B* **56**, R14243 (1997).
- ⁸ L. F. Feiner and A. M. Oleś, *Phys. Rev. B* **59**, 3295 (1999); N. N. Kovaleva, A. M. Oleś, A. M. Balbashov, A. Maljuk, D. N. Argyriou, G. Khaliullin, and B. Keimer, *ibid.* **81**, 235130 (2010).
- ⁹ W. Brzezicki, J. Dziarmaga, and A.M. Oleś, *Phys. Rev. Lett.* **109**, 237201 (2012); *Phys. Rev. B* **87**, 064407 (2013); W. Brzezicki and A.M. Oleś, *ibid.* **83**, 214408 (2011).
- ¹⁰ A. Kitaev and C. Laumann, arXiv:0904.2771 (2009).
- ¹¹ F. Trouselet, A.M. Oleś, and P. Horsch, *Europhys. Lett.* **91**, 40005 (2010); *Phys. Rev. B* **86**, 134412 (2012).
- ¹² A. Kitaev, *Annals of Physics* **321**, 2 (2006); G. Baskaran, S. Mandal, and R. Shankar, *Phys. Rev. Lett.* **98**, 247201 (2007); S.R. Hassan, P.V. Sriluckshmy, S.K. Goyal, R. Shankar, and D. Sénéchal, *ibid.* **110**, 037201 (2013).
- ¹³ S. Yan, D. A. Huse, and S. R. White, *Science* **332**, 1173 (2011).
- ¹⁴ L. Cincio and G. Vidal, *Phys. Rev. Lett.* **110**, 067208 (2013).
- ¹⁵ F. Verstraete and J. I. Cirac, arXiv:cond-mat/0407066v1 (2004).
- ¹⁶ D. Poilblanc, N. Schuch, D. Pérez-García, and J.I. Cirac, *Phys. Rev. B* **86**, 014404 (2012).
- ¹⁷ D. Poilblanc, N. Schuch, *Phys. Rev. B* **87**, 140407(R) (2013).
- ¹⁸ L. Wang, D. Poilblanc, Z.-C. Gu, X.-G. Wen, and F. Verstraete, *Phys. Rev. Lett.* **111**, 037202 (2013).
- ¹⁹ D. Poilblanc, P. Corboz, N. Schuch, and J. I. Cirac, arXiv:1404.5268.
- ²⁰ A.M. Oleś, L.F. Feiner, and J. Zaanen, *Phys. Rev. B* **61**, 6257 (2000).
- ²¹ M.V. Mostovoy and D.I. Khomskii, *Phys. Rev. Lett.* **92**, 167201 (2004).
- ²² M. A. Cazalilla, R. Citro, T. Giamarchi, E. Orignac, and M. Rigol, *Rev. Modern Phys.* **83**, 1405 (2011).
- ²³ A. G. Abanov, D. A. Ivanov, and Y. Qian, *J. Phys. A: Math. Theor.* **44**, 485001 (2011); P. Deift, P. A. Its, and I. Krasovsky, arXiv:0905.0443 (unpublished); T. Ehrhardt, *Operator Theory: Advances and Applications* **124**, 217-241 (2001).